Histologically Confirmed Diagnostic Efficacy of ^{18}F-rhPSMA-7 PET for N-Staging of Patients with Primary High-Risk Prostate Cancer

Markus Kroenke[1], Alexander Wurzer[2], Kristina Schwamborn[3], Lena Ulbrich[1], Lena Jooß[1], Tobias Maurer[4], Thomas Horn[5], Isabel Rauscher[1], Bernhard Haller[6], Michael Herz[1], Hans-Jürgen Wester[2], Wolfgang A. Weber[1], and Matthias Eiber[1]

[1]Department of Nuclear Medicine, School of Medicine, Klinikum rechts der Isar, Technical University of Munich, Munich, Germany; [2]Technical University of Munich, Munich, Germany; [3]Institute of Pathology, School of Medicine, Klinikum rechts der Isar, Technical University of Munich, Munich, Germany; [4]Martini-Klinik and Department of Urology, University Hospital Hamburg-Eppendorf, Hamburg, Germany; [5]Department of Urology, School of Medicine, Klinikum rechts der Isar, Technical University of Munich, Munich, Germany; and [6]Institute of Medical Informatics, Statistics and Epidemiology, School of Medicine, Technical University of Munich, Munich, Germany

^{18}F-rhPSMA-7 (radiohybrid prostate-specific membrane antigen [PSMA]) is a novel ligand for PET imaging. Here, we present data from a retrospective analysis using PET/CT and PET/MRI examinations to investigate the efficacy of ^{18}F-rhPSMA-7 PET for primary N-staging of patients with prostate cancer (PC) compared with morphologic imaging (CT or MRI) and validated by histopathology. **Methods:** Data from 58 patients with high-risk PC (according to the D'Amico criteria) who were staged with ^{18}F-rhPSMA-7 PET/CT or PET/MRI at our institution between July 2017 and June 2018 were reviewed. The patients had a median prescan prostate-specific antigen value of 12.2 ng/mL (range, 1.2–81.6 ng/mL). The median injected activity of ^{18}F-rhPSMA-7 was 327 MBq (range, 132–410 MBq), with a median uptake time of 79.5 min (range, 60–153 min). All patients underwent subsequent radical prostatectomy and extended pelvic lymph node dissection. The presence of lymph node metastases was determined by an experienced reader independently for both the PET and the morphologic datasets using a template-based analysis on a 5-point scale. Patient-level and template-based results were both compared with histopathologic findings. **Results:** Lymph node metastases were present in 18 patients (31.0%) and were located in 52 of 375 templates (13.9%). Receiver-operating-characteristic analyses showed ^{18}F-rhPSMA-7 PET to perform significantly better than morphologic imaging on both patient-based and template-based analyses (areas under curve, 0.858 vs. 0.649 [$P = 0.012$] and 0.765 vs. 0.589 [$P < 0.001$], respectively). On patient-based analyses, the sensitivity, specificity, and accuracy of ^{18}F-rhPSMA-7 PET were 72.2%, 92.5%, and 86.2%, respectively, and those of morphologic imaging were 50.0%, 72.5%, and 65.5%, respectively. On template-based analyses, the sensitivity, specificity, and accuracy of ^{18}F-rhPSMA-7 PET were 53.8%, 96.9%, and 90.9%, respectively, and those of morphologic imaging were 9.6%, 95.0%, and 83.2%, respectively. **Conclusion:** ^{18}F-rhPSMA-7 PET is superior to morphologic imaging for N-staging of high-risk primary PC. The efficacy of ^{18}F-rhPSMA-7 is similar to published data for ^{68}Ga-PSMA-11.

Received Aug. 8, 2019; revision accepted Dec. 3, 2019.
For correspondence or reprints contact: Matthias Eiber, Klinikum rechts der Isar, Ismaninger Straße 22, 81675 Munich, Germany.
E-mail: matthias.eiber@tum.de
Published online Dec. 13, 2019.

Key Words: hybrid imaging; lymph nodes; N-staging; PET; prostate cancer; prostate-specific membrane antigen (PSMA)

J Nucl Med 2020; 61:710–715
DOI: 10.2967/jnumed.119.234906

Prostate cancer (PC) is a leading cause of male cancer-related death worldwide (*1*). Determining the presence and extent of disease at primary diagnosis is important to accurately predict prognosis and to define the optimal treatment strategy *(2–4)*. Lymph node metastases may be detected in up to 25% of patients with PC and are correlated with the risk for recurrence and associated with overall survival (*5–7*).

The current gold standard for N-staging is pelvic lymphadenectomy, although this technique cannot evaluate regions outside the surgical field and is associated with morbidity and complications (*8,9*). Although cross-sectional imaging with CT, MRI, and PET with choline-based tracers is associated with low sensitivity (*10,11*), prostate-specific membrane antigen (PSMA)–ligand PET is increasingly used for primary staging of PC. It outperforms cross-sectional imaging (*12*) and has been reported to have a sensitivity in the range of 33%–99% and a consistently high specificity of over 90% (*13*).

^{18}F-labeled PSMA radiotracers are under clinical evaluation and offer several potential advantages such as a longer half-life, larger-batch production, and lower positron range than their ^{68}Ga-labeled counterparts. Promising results for primary staging have been demonstrated in a preliminary case series investigating ^{18}F-PSMA-1007 (*14*). Radiohybrid PSMA (rhPSMA) ligands are a new class of theranostic PSMA-targeting agents that can be efficiently labeled with ^{18}F and radiometals such as ^{68}Ga or ^{177}Lu (*15*). The lead compound in this class, ^{18}F-rhPSMA-7, shows favorable biodistribution with low bladder retention, fast kinetics, and encouraging first-in-men data (*16*).

The aim of this retrospective analysis was to evaluate the diagnostic performance of ^{18}F-rhPSMA-7 PET for primary N-staging of patients with high-risk PC compared with cross-sectional imaging and validated by histopathology.

MATERIALS AND METHODS

Patients

Data were retrospectively reviewed from all patients meeting the D'Amico criteria for high-risk PC (*17*) who underwent ^{18}F-rhPSMA-7 PET/CT or PET/MRI and subsequent radical prostatectomy and extended pelvic lymph node dissection at our clinic between July 2017 and June 2018. Patients were excluded if they had received neoadjuvant treatment (either before or after the PET scan) or had not undergone radical prostatectomy with extended pelvic lymphadenectomy at our institution. In total, 58 patients were enrolled (Fig. 1). Their characteristics are presented in Table 1.

All patients gave written informed consent for the anonymized evaluation and publication of their data. The analysis was approved by the local Ethics Committee (permit 290/18S). Administration of ^{18}F-rhPSMA-7 complied with the German Medicinal Products Act, AMG §13 2b, and the responsible regulatory body (government of Oberbayern).

^{18}F-rhPSMA-7 Synthesis, Administration, and PET Imaging

^{18}F-rhPSMA-7 was synthesized as reported previously (*15*). ^{18}F-rhPSMA-7 (median activity, 327 MBq; range 132–410 MBq) was administered as an intravenous bolus a median of 79.5 min (range, 60–153 min) before scanning. Thirty-nine patients underwent contrast-enhanced ^{18}F-rhPSMA-7 PET/CT (Biograph mCT Flow; Siemens Medical Solutions). Nineteen patients underwent ^{18}F-rhPSMA-7 PET/MRI (Biograph mMR; Siemens Medical Solutions). The PET/CT and PET/MRI acquisitions were conducted as described previously (*18,19*). All patients received diluted oral contrast medium (300 mg of ioxitalamate [Telebrix; Guerbet]).

All PET scans were acquired in 3-dimensional mode with an acquisition time of 2 min per bed position in flow technique (equals 1.1 mm/s) for PET/CT and 4 min per bed position for PET/MRI. Emission data were corrected for randoms, dead time, scatter, and attenuation and were reconstructed iteratively by an ordered-subsets expectation maximization algorithm (4 iterations, 8 subsets) followed by a postreconstruction smoothing gaussian filter (5 mm in full width at half maximum).

Image Analysis

All ^{18}F-rhPSMA-7 PET/CT and PET/MRI datasets were reviewed by 2 experienced individuals (a board-certified radiologist and nuclear medicine specialist and a board-certified nuclear medicine specialist) who were masked to the postoperative histology results. The results were determined by consensus. In a first step, the anatomic data using the diagnostic contrast-enhanced CT dataset (PET/CT examinations)

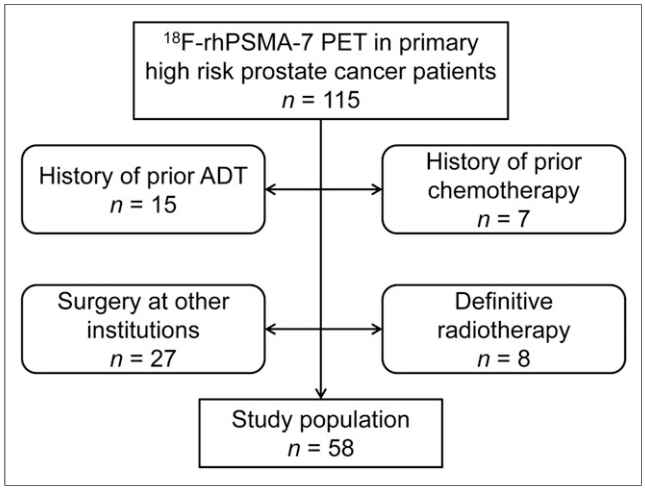

FIGURE 1. Flowchart for patient selection.

TABLE 1
Patient Characteristics

Characteristic	Data
Total patients (*n*)	58 (100%)
Age at imaging (y)	
Mean	67.7
Median	68
IQR	65–73
Range	48–80
PSA at imaging (ng/mL)	
Mean	18.1
Median	12.2
IQR	7.3–22.4
Range	1.2–81.6
Gleason score (*n*)	
7a	11 (19.0%)
7b	25 (43.1%)
8	4 (6.9%)
9	18 (31.0%)
10	0
Pathologic T-stage (*n*)	
≤pT2c	26 (44.8%)
pT3a	12 (20.7%)
≥pT3b	20 (34.5%)
Pathologic N-stage (*n*)	
pN0	40 (69%)
pN1	18 (31%)
Lymph nodes removed (*n*)	
Total	1,137
Median	18
IQR	8
Range	8–53
Lymph nodes with metastasis (*n*)	
Total	71
Median	0
IQR	1
Range	0–15
Injected activity (MBq)	
Mean	327.7
Median	327
IQR	306.5–363
Range	132–410
Uptake time (min)	
n	82
Median	79.5
IQR	70–87.25
Range	60–153

IQR = interquartile range; PSA = prostate-specific antigen.

and the pelvic axial T2-weighted turbo spin-echo and the whole-body axial T2-weighted half-Fourier single-shot turbo spin-echo sequences (PET/MRI examinations) were analyzed. In a second step, after at least 4 wk, a second read of the corresponding ^{18}F-rhPSMA-7 PET scan was performed. For the latter, anatomic images were used only for anatomic allocation of a suggestive focus of increased uptake to the corresponding lymph node template. In both reading sessions, each template was rated in PET and in CT or MRI using a 5-point Likert scale.

For PET, the following criteria were used: a rating of 1 indicated tumor manifestation (intense, focal ^{18}F-rhPSMA-7 uptake higher than uptake in liver); 2, probable tumor manifestation (^{18}F-rhPSMA-7 uptake clearly higher than the background level in vessels but not higher than liver); 3, equivocal findings (^{18}F-rhPSMA-7 faint uptake between the background level in muscle and the background level in vessels); 4, probable benign findings (^{18}F-rhPSMA-7 uptake as faint as the background level, e.g., equal to the level in adjacent muscle); and 5, benign findings (no ^{18}F-rhPSMA-7 uptake). In the PET rating, anatomic images were used only for anatomic allocation of a suggestive focus of increased uptake to the corresponding lymph node field.

For morphologic imaging, the following criteria were used: a rating of 1 indicated tumor manifestation (short-axis diameter $>$ 10mm); 2, probable tumor manifestation (short-axis diameter of 8–10 mm, a round configuration, and a regional grouping); 3, equivocal findings (short-axis diameter of 8–10 mm, an oval configuration, and no regional grouping); 4, probable benign findings (short-axis diameter $<$ 8 mm); and 5, benign findings (short-axis diameter $<$ 5mm).

Histopathology

During surgery, extended pelvic lymphadenectomy was performed as previously described (*20,21*). The following standard lymph node templates were collected separately: right/left common iliac vessel, right/left internal iliac vessel, right/left external iliac vessel, and right/left obturator fossa. When preoperative imaging showed ^{18}F-rhPSMA-7 PET–positive lymph nodes outside these regions, additional templates (e.g., presacral/pararectal) were resected. The uropathologists were not aware of the preoperative imaging results.

Statistical Analysis

The histopathologic results from resected lymph nodes were correlated with the results of cross-sectional imaging (MRI or CT) and ^{18}F-rhPSMA-7 PET in a patient- and template-based manner.

The overall diagnostic accuracy of patient-level data was assessed using receiver-operating-characteristic (ROC) analyses. ROC curves were calculated for both modalities (^{18}F-rhPSMA-7 PET and morphologic imaging). Areas under the ROC curves (AUCs) with 95% confidence intervals (CIs) were calculated and compared with each other. For patient-based analysis, the method of DeLong et al. (*22*) was used, and the approach proposed by Obuchowski (*23*) was considered for template-based analyses to account for correlations of multiple assessments within 1 patient.

To estimate sensitivities, specificities, and accuracies, a dichotomization of the semiquantitative 5-scale rating for PET and for CT or MRI was performed to conduct statistical analyses. The Youden index (sensitivity + specificity − 1) was used to determine the best cutoff for this analysis. In the patient-based analyses, exact CIs were estimated for these measures on the basis of the binomial distribution (Clopper–Pearson intervals). For the template-based analyses, logistical generalized-estimating-equation models were fitted to the data to account for the correlation of multiple observations within the same patient (*24,25*). For estimation of sensitivities with associated CIs, only templates with a positive histologic result were included, and the result of the diagnostic test was used as a dependent variable.

To derive estimates for the specificities, a variable indicating whether a negative test result was observed was used as a dependent variable, and only patients with a negative histopathologic result were included. Accuracy was estimated in an intercept-only model with a dependent variable that indicated whether the test result and the result of the histopathologic assessment agreed. For the generalized-estimating-equation model, an independent correlation structure was assumed. A significance level of 5% was considered for all tests. All statistical analyses were performed using the statistical software R (*26*), with its packages pROC (*27*) and geepack (*28*).

RESULTS

Histopathologic Results and ROC Analysis

Lymph node metastases were present in 52 of 375 resected templates (13.9%) in 18 of the 58 patients (31%). ^{18}F-rhPSMA-7 PET revealed positivity of the local tumor in 57 patients (98.3%). One patient showed evidence of distant lymph node metastases and bone metastases (1.9%).

On patient-based analysis, ROC curves showed an AUC of 0.858 (95% CI, 0.739–0.978) for ^{18}F-rhPSMA-7 PET and 0.649 (95% CI, 0.492–0.805) for morphologic imaging, for the detection of lymph node metastases (Fig. 2A). On template-based analysis, ROC curves showed an AUC of 0.766 (95% CI, 0.697–0.834) for ^{18}F-rhPSMA-7 PET and 0.589 (95% CI, 0.522–0.656) for morphologic imaging alone (Fig. 2B). ^{18}F-rhPSMA-7 PET performed significantly better than morphologic imaging alone on patient-based analysis (difference in AUCs, 0.210; 95% CI, 0.046–0.373; P = 0.012) and template-based analysis (difference in AUCs, 0.177; 95% CI, 0.104–0.249; $P < 0.001$).

For morphologic imaging, a score of 1, 2, or 3 on the Likert scale was regarded as positive, whereas a score of 4 or 5 was considered negative, on the basis of the Youden index. For ^{18}F-rhPSMA-7 PET, a score of 1 or 2 was compared with a score of 3, 4, or 5. A representative example is presented in Figure 3.

Diagnostic Performance on Patient-Based Analysis

Compared with histopathology, ^{18}F-rhPSMA-7 PET detected 13 of 18 patients with histologically proven lymph node metastasis (sensitivity, 72.2%; 95% CI, 46.5%–90.3%) whereas 3 of 40 patients without lymph node metastases were positive on ^{18}F-rhPSMA-7 PET (specificity, 92.5%; 95% CI, 79.6%–98.4%). In total, ^{18}F-rhPSMA-7 PET showed an accuracy of 86.2% (95% CI, 74.6%–93.9%) on patient-based analysis (Table 2).

Morphologic imaging alone correctly classified 9 of 18 patients as positive and 29 of 40 patients as negative for lymph node metastases, resulting in a sensitivity of 50.0% (95% CI, 26.0%–74.0%), a specificity of 72.5% (95% CI, 56.1%–85.4%), and an accuracy of 65.5% (95% CI, 51.9%–77.5%) (Table 2).

PET and morphologic imaging revealed concordant correct results (both true-positive and true-negative) in 35 of 58 patients (60.3%) and concordant false results in 5 (8.6%). Discordant results were obtained in 18 patients (31%). Histologic evaluation revealed that PET imaging gave true-positive and true-negative results in 15 of these 18 patients (83.3%) with discordant results. ^{18}F-rhPSMA-7 PET reported both fewer false-positives and fewer false-negatives than morphologic imaging (3 vs. 11 patients and 5 vs. 9 patients, respectively).

Diagnostic Performance on Template-Based Analysis

Compared with histopathology, ^{18}F-rhPSMA-7 PET detected 28 of 52 templates with histologically proven lymph node metastasis (sensitivity, 53.8%; 95% CI, 41.3%–66.0%), whereas 10 of 323 templates without lymph node metastases were positive on ^{18}F-rhPSMA-7 PET (specificity, 96.9%; 95% CI, 91.4%–98.9%). In total, ^{18}F-rhPSMA-7 PET showed an accuracy of 90.9% (95% CI, 85.7%–94.4%) on a template-based analysis (Table 3).

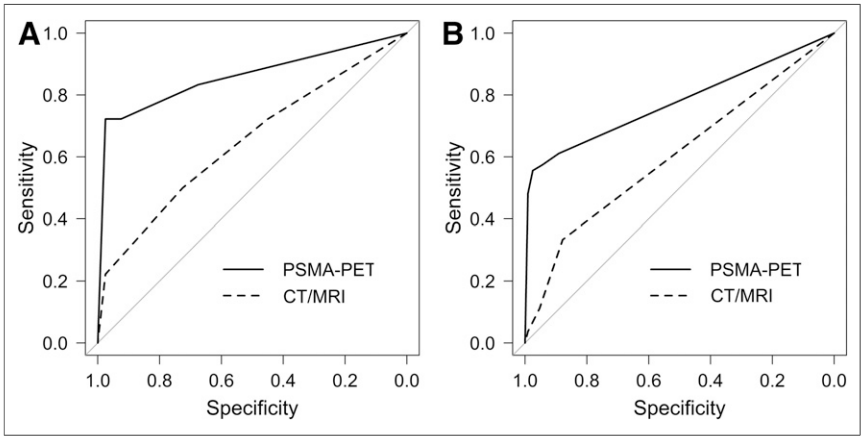

FIGURE 2. ROC curves for ^{18}F-rhPSMA-7 PET and morphologic imaging (MRI/CT) for primary lymph node staging of prostate cancer in patient-based analysis (A) and template-based analysis (B). Comparison to AUC of 0.5 is indicated by gray line.

Cross-sectional imaging alone correctly classified 5 of 52 templates as positive and 307 of 323 templates as negative for lymph node metastases, resulting in a sensitivity of 9.6% (95% CI, 4.5%–19.3%), a specificity of 95.0% (95% CI, 92.2%–96.9%), and an accuracy of 83.2% (95% CI, 76.5%–88.3%) (Table 3).

The median size of the lymph node metastases not detected by ^{18}F-rhPSMA-7 PET was 4.5 mm (range, 0.3–15 mm). In 2 patients, the histopathologically false-positive results of ^{18}F-rhPSMA-7 PET were challenged.

Follow-up data retrieved from the postoperative clinical course for 2 patients revealed that lymph node templates that had been assigned as false-positives with^{18}F-rhPSMA-7 PET were in fact true-positives. In 1 patient with a persistently elevated level of prostate-specific antigen postoperatively, subsequent imaging 4 mo later revealed persistent PSMA-ligand positivity in the initial region. A subsequent second targeted lymphadenectomy found a lymph node metastasis (Supplemental Fig. 1; supplemental materials are available at http://jnm.snmjournals.org). In a second patient, radiation planning (4 mo after the scan and after the operation) showed that the lesions in the right obturator and left common iliac lymph nodes had not been removed but decreased in size, most likely because of the start of androgen deprivation therapy after surgery. Updated statistics corrected for this information are presented in Supplemental Table 2.

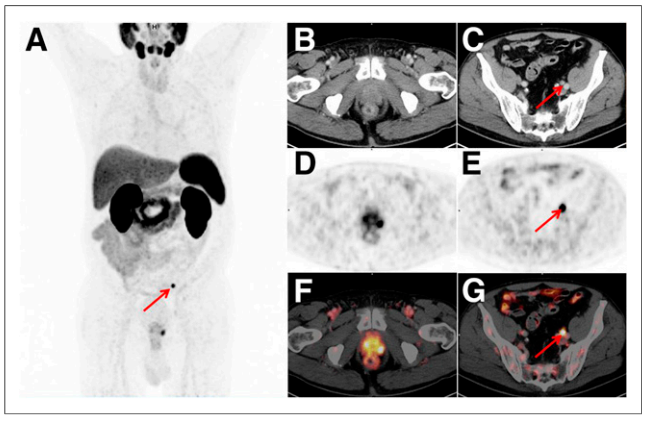

FIGURE 3. Set of images from 71-y-old patient (Gleason score of 10, initial prostate-specific antigen level of 1.15 ng/mL). (A) Whole-body maximum-intensity projection displays local tumor and 1 suspected lesion (arrow). Local tumor is not detectable on CT (B) but shows increased tracer uptake on ^{18}F-rhPSMA-7 PET (D) and PET/CT (F). CT (E) reveals suggestive finding (arrow), with 8-mm lymph node ventral to left external iliac vein; corresponding ^{18}F-rhPSMA-7 PET (E) and PET/CT images (G) show intense uptake with high lesion-to-background ratio in this small lymph node, indicating lymph node metastasis. Radical prostatectomy with extended pelvic lymph node dissection confirmed single lymph node metastasis.

DISCUSSION

The results of this retrospective analysis indicate that PET with the novel PSMA ligand ^{18}F-rhPSMA-7 shows high diagnostic accuracy for N-staging in patients with primary high-risk PC. Its efficacy is superior to that of morphologic imaging, which is recommended by most guidelines (*3*).

Accurate localization of lesions, particularly to lymph nodes in patients with high-risk PC, is essential to optimize treatment planning. In particular, the identification of lymph node metastases is an unmet clinical need for noninvasive imaging given its adverse prognostic implications (*4*). Morphologic imaging, using CT and MRI, has high variability in diagnostic performance for lymph node metastases (*29*). Characterization of lymph nodes solely by size is of limited use, as up to 80% of metastatic lymph nodes are normal-sized (<8 mm) (*30,31*). Moreover, PET with ^{11}C- or ^{18}F-labeled choline derivatives is not recommended for first-line staging in patients with intermediate- to high-risk PC (*3*).

TABLE 2
Patient-Based Diagnostic Accuracy of Cross-Sectional Imaging and ^{18}F-rhPSMA-7 PET Compared with Histologic Findings for Lymph Node Metastasis

Morphology*			^{18}F-rhPSMA7-PET†		
	Histology			Histology	
Grade	Positive	Negative	Grade	Positive	Negative
1	4	1	1	13	1
2	0	0	2	0	2
3	5	10	3	1	5
4	4	11	4	1	5
5	5	18	5	3	27
Total	18	40	Total	18	40

*Grades 1–3 are positive (positive predictive value, 72.5%) and grades 4 and 5 negative (negative predictive value, 76.3%) for LN metastasis based on highest Youden index. Sensitivity is 50.0%, specificity is 72.5%, and accuracy is 65.5%.

†Grades 1 and 2 are positive (positive predictive value, 81.3%) and grades 3–5 negative (negative predictive value, 88.1%) for LN metastasis based on highest Youden index. Sensitivity is 72.2%, specificity is 92.5%, and accuracy is 86.2%.

TABLE 3
Template-Based Diagnostic Accuracy of Cross-Sectional Imaging and ^{18}F-rhPSMA-7 PET Compared with Histologic Findings for Lymph Node Metastasis

Morphology*			^{18}F-rhPSMA7-PET†		
	Histology			Histology	
Grade	Positive	Negative	Grade	Positive	Negative
1	1	4	1	24	5
2	0	0	2	4	5
3	4	12	3	1	10
4	11	25	4	2	17
5	36	282	5	21	286
Total	52	323	Total	52	323

*Grades 1–3 are positive (positive predictive value, 28.8%) and grades 4 and 5 negative (negative predictive value, 86.7%) for LN metastasis based on highest Youden index. Sensitivity is 9.6%, specificity is 95.0%, and accuracy is 83.2%.

†Grades 1 and 2 are positive (positive predictive value, 73.7%) and grades 3–5 negative (negative predictive value, 92.9%) for LN metastasis based on highest Youden index. Sensitivity is 53.8%, specificity is 96.9%, and accuracy is 90.9%.

Currently, PSMA ligands are increasingly used in PC work-up. They specifically target PC cells irrespective of their metabolic state (*32*) and offer a favorable lesion-to-background ratio for detection of metastatic lymph nodes, as normal lymphatic or retroperitoneal fatty tissue does not express PSMA.

The present results clearly indicate that ^{18}F-rhPSMA-7 PET performs significantly better than morphologic imaging techniques. This difference is even more pronounced in the template-based analysis, in which the sensitivity of morphologic imaging dropped to 9.6% (95% CI, 4.5%–19.3%). The accuracy of ^{18}F-rhPSMA-7 PET was 86% and 91%, versus 66% and 83% for morphologic imaging, for patient- and template-based analyses, respectively.

Compared with ^{68}Ga-PSMA-11, ^{18}F-rhPSMA-7 seems to perform equally well. In a subcohort of 88 high-risk patients, Maurer et al. reported a sensitivity, specificity, and accuracy of 67%, 98%, and 84%, respectively, compared with 72%, 93%, and 86% for ^{18}F-rhPSMA-7 (*33*). Several metaanalyses have summarized published data on the performance of ^{68}Ga-PSMA-11 for N-staging; Hope et al. summarized data from 266 patients for initial staging and reported a sensitivity, specificity, positive predictive value, negative predictive value, and accuracy of 74%, 96%, 93%, 85%, and 86%, respectively (*34*). Corfield et al. (*12*) reported ranges for sensitivity, specificity, negative predictive value, and positive predictive value of 33%–92%, 64%–91%, 83%–96%, and 80%–96%, respectively, across their analysis of over 200 patients. Similar pooled data have been published by von Eyben et al. (*35*) and Perera et al. (*13*). Despite a considerable range in sensitivity in the reported studies, specificity was consistently high in nearly all reports (Supplemental Table 1), as was observed in the current analysis for ^{18}F-rhPSMA-7. Only a limited comparison with other ^{18}F-labeled PSMA ligands is possible because of a paucity of published data. For ^{18}F-DCFPyl, Gorin et al. reported data from a small prospective evaluation of 25 patients—a sensitivity and specificity of 71.4% (95% CI, 29.0–96.3) and 88.9% (95% CI, 65.3–98.6), respectively (*36*). It is noteworthy that in our study the specificity on the template-based analysis was slightly underestimated because 2 templates designated as false-positive were in fact true-positive as indicated by follow-up data (adjusted statistics in Supplemental Table 2). The problem of incomplete resection of even preoperatively known lymph node metastases has been recently reported (*37*). A potential solution could be the application of radioguided surgery as known in recurrent disease (*38*).

Notably in our study, nearly all patients (98.3%; 57/58) expressed high ^{18}F-rhPSMA-7 uptake in the local tumor. One patient with a negative primary tumor was not found to have any lymph node metastases by histopathology. As known from ^{68}Ga-PSMA-11, size is critical for lesion detection (*39*). In the present data, the mean size of negative lymph node templates is similar to that previously reported by Maurer et al. (3.5 mm) (*33*).

The novel PSMA ligand ^{18}F-rhPSMA-7 offers several advantages over more established PSMA-based tracers, such as ^{68}Ga-PSMA-11, and has already shown encouraging data for detection efficacy in biochemical recurrence (*40*). The considerably longer half-life of 110 min yields the advantages of easier handling and potential wide-range distribution due to large-scale cyclotron-based production of ^{18}F. Furthermore, spatial resolution might be improved by a lower positron range (*41*). However, compared with literature on ^{68}Ga-PSMA-11, our results do not reveal significant diagnostic improvements. Nevertheless, compared with ^{18}F-PSMA-1007 and ^{18}F-DCFPyl, potential benefits may arise from the radiohybrid concept, facilitating the use of ^{68}Ga and therapeutic nuclides that offer not only ^{68}Ga-based imaging for remote locations using a generator but also the ability to exploit applications for theranostics (e.g., exact pretherapy PET dosimetry for treatment planning).

Our analysis has limitations. First, it was retrospective and on a limited number of patients. Second, we had to restrict it to a template-based approach, as single lymph node correlations between imaging and surgery are not feasible. However, the analysis was performed in a rigorous fashion and provided substantial evidence for future prospective trials. Third, PSMA immunohistochemistry was not performed for lymph node metastases. However, for N-staging, routine hematoxylin and eosin staining is usually sufficient. Only in cases of a second primary tumor would PSMA immunohistochemistry be helpful to investigate its etiology. Fourth, as this analysis was primarily intended to investigate the potential of ^{18}F-rhPSMA-7 for N-staging, no detailed analysis of its potential for describing the intraprostatic tumor extent or distant disease was performed. Fifth, given that only patients who subsequently underwent surgery were included in the study, the potential of ^{18}F-rhPSMA-7 to detect organ (e.g., bone) metastases could not be investigated in this analysis.

CONCLUSION

N-staging of high-risk primary PC with ^{18}F-rhPSMA-7 PET is superior to that with morphologic imaging. The efficacy of ^{18}F-rhPSMA-7 is similar to that of published data for ^{68}Ga-PSMA-11 and offers the additional logistical and economic advantages of radiofluorination.

DISCLOSURE

Hans-Jürgen Wester, Alexander Wurzer, and Matthias Eiber are named as inventors on a patent application for rhPSMA. Hans-Jürgen Wester and Matthias Eiber received funding from the SFB 824 (DFG Sonderforschungsbereich 824, project B11) from the Deutsche Forschungsgemeinschaft, Bonn, Germany, and from Blue Earth Diagnostics Ltd. (licensee for rhPSMA) as part of an

academic collaboration. Hans-Jürgen Wester is a founder, shareholder, and advisory board member of Scintomics GmbH, Fuerstenfeldbruck, Germany. Matthias Eiber and Wolfgang Weber are consultants for Blue Earth Diagnostics Ltd. No other potential conflict of interest relevant to this article was reported.

KEY POINTS

QUESTION: What is the diagnostic efficacy of ^{18}F-rhPSMA-7 in N-staging of high-risk PC in the primary setting?

PERTINENT FINDINGS: Compared with morphologic imaging, ^{18}F-rhPSMA-7 PET provides superior N-staging of high-risk primary PC. The efficacy of ^{18}F-rhPSMA-7 is similar to that of published data for ^{68}Ga-PSMA-11 and offers the additional logistical and economic advantages of radiofluorination.

IMPLICATIONS FOR PATIENT CARE: ^{18}F-rhPSMA-7 PET can benefit patients by significantly improving primary N-staging.

REFERENCES

1. Torre LA, Bray F, Siegel RL, Ferlay J, Lortet-Tieulent J, Jemal A. Global cancer statistics, 2012. *CA Cancer J Clin.* 2015;65:87–108.
2. Cheng L, Zincke H, Blute ML, Bergstralh EJ, Scherer B, Bostwick DG. Risk of prostate carcinoma death in patients with lymph node metastasis. *Cancer.* 2001;91:66–73.
3. Mottet N, Bellmunt J, Bolla M, et al. EAU-ESTRO-SIOG guidelines on prostate cancer: part 1—screening, diagnosis, and local treatment with curative intent. *Eur Urol*. 2017;71:618–629.
4. Kothari PS, Scardino PT, Ohori M, Kattan MW, Wheeler TM. Incidence, location, and significance of periprostatic and periseminal vesicle lymph nodes in prostate cancer. *Am J Surg Pathol.* 2001;25:1429–1432.
5. Danella JF, deKernion JB, Smith RB, Steckel J. The contemporary incidence of lymph node metastases in prostate cancer: implications for laparoscopic lymph node dissection. *J Urol.* 1993;149:1488–1491.
6. Partin AW, Mangold LA, Lamm DM, Walsh PC, Epstein JI, Pearson JD. Contemporary update of prostate cancer staging nomograms (Partin tables) for the new millennium. *Urology.* 2001;58:843–848.
7. Gervasi LA, Mata J, Easley JD, et al. Prognostic significance of lymph nodal metastases in prostate cancer. *J Urol.* 1989;142:332–336.
8. Campbell SC, Klein EA, Levin HS, Piedmonte MR. Open pelvic lymph node dissection for prostate cancer: a reassessment. *Urology.* 1995;46:352–355.
9. Briganti A, Blute ML, Eastham JH, et al. Pelvic lymph node dissection in prostate cancer. *Eur Urol.* 2009;55:1251–1265.
10. Briganti A, Abdollah F, Nini A, et al. Performance characteristics of computed tomography in detecting lymph node metastases in contemporary patients with prostate cancer treated with extended pelvic lymph node dissection. *Eur Urol.* 2012;61:1132–1138.
11. Evangelista L, Guttilla A, Zattoni F, Muzzio PC, Zattoni F. Utility of choline positron emission tomography/computed tomography for lymph node involvement identification in intermediate- to high-risk prostate cancer: a systematic literature review and meta-analysis. *Eur Urol.* 2013;63:1040–1048.
12. Corfield J, Perera M, Bolton D, Lawrentschuk N. ^{68}Ga-prostate specific membrane antigen (PSMA) positron emission tomography (PET) for primary staging of high-risk prostate cancer: a systematic review. *World J Urol.* 2018;36:519–527.
13. Perera M, Papa N, Christidis D, et al. Sensitivity, specificity, and predictors of positive ^{68}Ga-prostate-specific membrane antigen positron emission tomography in advanced prostate cancer: a systematic review and meta-analysis. *Eur Urol.* 2016;70:926–937.
14. Giesel FL, Hadaschik B, Cardinale J, et al. F-18 labelled PSMA-1007: biodistribution, radiation dosimetry and histopathological validation of tumor lesions in prostate cancer patients. *Eur J Nucl Med Mol Imaging.* 2017;44:678–688.
15. Wurzer A, Di Carlo D, Schmidt A, et al. Radiohybrid ligands: a novel tracer concept exemplified by ^{18}F- or ^{68}Ga-labeled rhPSMA-inhibitors. *J Nucl Med.* 2020;61:735–742.
16. Oh SW, Wurzer A, Teoh EJ, et al. Quantitative and qualitative analyses of biodistribution and PET image quality of a novel radiohybrid PSMA, ^{18}F-rhPSMA-7, in patients with prostate cancer. *J Nucl Med.* 2020;61:702–709.
17. D'Amico AV, Whittington R, Malkowicz SB, et al. Biochemical outcome after radical prostatectomy, external beam radiation therapy, or interstitial radiation therapy for clinically localized prostate cancer. *JAMA.* 1998;280:969–974.
18. Souvatzoglou M, Eiber M, Martinez-Moeller A, et al. PET/MR in prostate cancer: technical aspects and potential diagnostic value. *Eur J Nucl Med Mol Imaging.* 2013;40(suppl 1):S79–S88.
19. Eiber M, Maurer T, Souvatzoglou M, et al. Evaluation of hybrid ^{68}Ga-PSMA ligand PET/CT in 248 patients with biochemical recurrence after radical prostatectomy. *J Nucl Med.* 2015;56:668–674.
20. Heck MM, Retz M, Bandur M, et al. Topography of lymph node metastases in prostate cancer patients undergoing radical prostatectomy and extended lymphadenectomy: results of a combined molecular and histopathologic mapping study. *Eur Urol.* 2014;66:222–229.
21. Maurer T, Souvatzoglou M, Kubler H, et al. Diagnostic efficacy of [^{11}C]choline positron emission tomography/computed tomography compared with conventional computed tomography in lymph node staging of patients with bladder cancer prior to radical cystectomy. *Eur Urol.* 2012;61:1031–1038.
22. DeLong ER, DeLong DM, Clarke-Pearson DL. Comparing the areas under two or more correlated receiver operating characteristic curves: a nonparametric approach. *Biometrics.* 1988;44:837–845.
23. Obuchowski NA. Nonparametric analysis of clustered ROC curve data. *Biometrics.* 1997;53:567–578.
24. Smith PJ, Hadgu A. Sensitivity and specificity for correlated observations. *Stat Med.* 1992;11:1503–1509.
25. Zeger SL, Liang KY. Longitudinal data analysis for discrete and continuous outcomes. *Biometrics.* 1986;42:121–130.
26. The R project for statistical computing. R website. https://www.R-project.org/. Accessed January 8, 2020.
27. Robin X, Turck N, Hainard A, et al. pROC: an open-source package for R and S+ to analyze and compare ROC curves. *BMC Bioinformatics.* 2011;12:77.
28. Halekoh U, Hojsgaard S, Yan J. The R package geepack for generalized estimating equations. *J Stat Softw.* 2006;15:1–11.
29. Hövels AM, Heesakkers RA, Adang EM, et al. The diagnostic accuracy of CT and MRI in the staging of pelvic lymph nodes in patients with prostate cancer: a meta-analysis. *Clin Radiol.* 2008;63:387–395.
30. Tiguert R, Gheiler EL, Tefilli MV, et al. Lymph node size does not correlate with the presence of prostate cancer metastasis. *Urology.* 1999;53:367–371.
31. Heesakkers RA, Hovels AM, Jager GJ, et al. MRI with a lymph-node-specific contrast agent as an alternative to CT scan and lymph-node dissection in patients with prostate cancer: a prospective multicohort study. *Lancet Oncol.* 2008;9:850–856.
32. Afshar-Oromieh A, Haberkorn U, Eder M, Eisenhut M, Zechmann CM. [^{68}Ga] gallium-labelled PSMA ligand as superior PET tracer for the diagnosis of prostate cancer: comparison with ^{18}F-FECH. *Eur J Nucl Med Mol Imaging.* 2012;39:1085–1086.
33. Maurer T, Gschwend JE, Rauscher I, et al. Diagnostic efficacy of ^{68}gallium-PSMA positron emission tomography compared to conventional imaging for lymph node staging of 130 consecutive patients with intermediate to high risk prostate cancer. *J Urol.* 2016;195:1436–1443.
34. Hope TA, Goodman JZ, Allen IE, Calais J, Fendler WP, Carroll PR. Meta-analysis of ^{68}Ga-PSMA-11 PET accuracy for the detection of prostate cancer validated by histopathology. *J Nucl Med.* 2019;60:786–793.
35. von Eyben FE, Picchio M, von Eyben R, Rhee H, Bauman G. ^{68}Ga-labeled prostate-specific membrane antigen ligand positron emission tomography/computed tomography for prostate cancer: a systematic review and meta-analysis. *Eur Urol Focus.* 2018;4:686–693.
36. Gorin MA, Rowe SP, Patel HD, et al. Prostate specific membrane antigen targeted ^{18}F-DCFPyL positron emission tomography/computerized tomography for the preoperative staging of high risk prostate cancer: results of a prospective, phase II, single center study. *J Urol.* 2018;199:126–132.
37. Farolfi A, Gafita A, Calais J, et al. ^{68}Ga-PSMA-11 positron emission tomography detects residual prostate cancer after prostatectomy in a multicenter retrospective study. *J Urol.* 2019;202:1174–1181.
38. Maurer T, Robu S, Schottelius M, et al. ^{99m}Technetium-based prostate-specific membrane antigen-radioguided surgery in recurrent prostate cancer. *Eur Urol.* 2019;75:659–666.
39. Jilg CA, Drendel V, Rischke HC, et al. Diagnostic accuracy of Ga-68-HBED-CC-PSMA-ligand-PET/CT before salvage lymph node dissection for recurrent prostate cancer. *Theranostics.* 2017;7:1770–1780.
40. Eiber M, Kroenke N, Wurzer A, et al. ^{18}F-rhPSMA-7 PET for the detection of biochemical recurrence of prostate cancer after radical prostatectomy. *J Nucl Med.* 2020;61:696–701.
41. Cho ZH, Chan JK, Ericksson L, et al. Positron ranges obtained from biomedically important positron-emitting radionuclides. *J Nucl Med.* 1975;16:1174–1176.